Acousto-electric tomography

Hao Zhang, Lihong V. Wang

Hao Zhang, Lihong V. Wang, "Acousto-electric tomography," Proc. SPIE 5320, Photons Plus Ultrasound: Imaging and Sensing, (12 July 2004); doi: 10.1117/12.532610

SPIE.

Event: Biomedical Optics 2004, 2004, San Jose, CA, United States

Acousto-electric tomography

Hao Zhang and Lihong V. Wang*
Optical Imaging Laboratory, Department of Biomedical Engineering
Texas A&M University, 3120 TAMU, College Station, Texas 77843-3120

ABSTRACT

Although the electric impedance of biological tissues is highly sensitive to their physiological and pathological status, pure electrical impedance tomography (EIT) has very poor spatial resolution. We invented acousto-electric tomography (AET) to image the electric impedance properties of biological tissues with high spatial resolution. AET is based on acousto-electric modulation, which is the localized variation in conductivity produced by a focused ultrasonic wave. It combines the contrast advantage of EIT and the resolution advantage of ultrasound imaging. The spatial resolution of AET is primarily defined by the size of the ultrasonic focal spot. Therefore, the resolution is much better than that of EIT, and it is scalable with the acoustic parameters. The contrast of AET is determined by the combination of three factors: the electric impedance, the media dependent modulation coefficient, and the acoustic properties. Unlike EIT, AET forms images directly without resorting to inverse algorithms. And unlike traditional ultrasonography, AET is free of speckles.
Keywords: Acousto-electric modulation, ultrasound, electric impedance, tomography

1. INTRODUCTION

X-ray mammography and ultrasonography are the most widely used imaging modalities in early breast cancer detection, and X-ray mammography has long been considered the "Gold Standard." However, X-ray mammography uses ionizing radiation and its contrast is less than 2 [1]. Ultrasound also has limited contrast in soft tissue, especially in early stage tumors. But the contrast in the electric impedance property of cancerous tissue relative to that of normal tissue can be up to 40 [2]. Electrical impedance tomography (EIT), also referred to as applied potential tomography, produces images of the electric impedance distribution in a body by means of noninvasive electrical measurements and a reconstruction algorithm. Although EIT has been investigated for decades [3]–[5], the inherent limitations of its spatial resolution, which have been demonstrated both experimentally [6] and theoretically [7], have prevented its widespread application. Ultrasound imaging provides good resolution, but its speckle artifacts have limited its applications as well.

A hybrid method, which combines electric impedance contrast and ultrasonic resolution, may potentially be the ideal solution to the above problems. We present one such new approach here. Acousto-electric tomography (AET) is able to image electric impedance properties with significantly improved spatial resolution using a direct image formation method. AET is based on acousto-electric (AE) modulation which has been recently investigated recently [8]–[10]. A focused ultrasonic wave causes changes in pressure when traveling in a medium. Therefore, a volume occupied by an ultrasonic beam column experiences periodic cycles of mechanical compression and rarefaction that are determined by the ultrasonic frequency. AE modulation occurs only within this volume, and, therefore, it is spatially encoded. The propagation of the ultrasound induces changes in conductivity, $\Delta\sigma$, and this effect has been approximated as [10]

$$\Delta\sigma = \sigma L P , \qquad (1)$$

where σ is the conductivity of the media; L is a medium dependent modulation coefficient; and P is the applied ultrasonic pressure. Variation in the conductivity causes variation in the electric impedance, which can then be detected from the object's surface. If the same focused acoustic field is scanned across the object, the modulation reflects only local properties, and the modulation strength versus the associated locations of the ultrasonic beam forms an image.

* To whom all correspondence should be addressed. Telephone: 979-847-9040; fax: 979-845-4450; electronic mail: LWang@tamu.edu; URL: http://oilab.tamu.edu.

Photons Plus Ultrasound: Imaging and Sensing, edited by
Alexander A. Oraevsky, Lihong V. Wang, Proceedings of SPIE Vol. 5320
(SPIE, Bellingham, WA, 2004) 1605-7422/04/$15 · doi: 10.1117/12.532610

This paper describes the invention of AET and presents images from both saline-rubber phantoms and biological tissue samples. The system resolution has been quantified by acquiring a line-spread function (LSF) and the contrast mechanism has been demonstrated by imaging a gel-gel phantom.

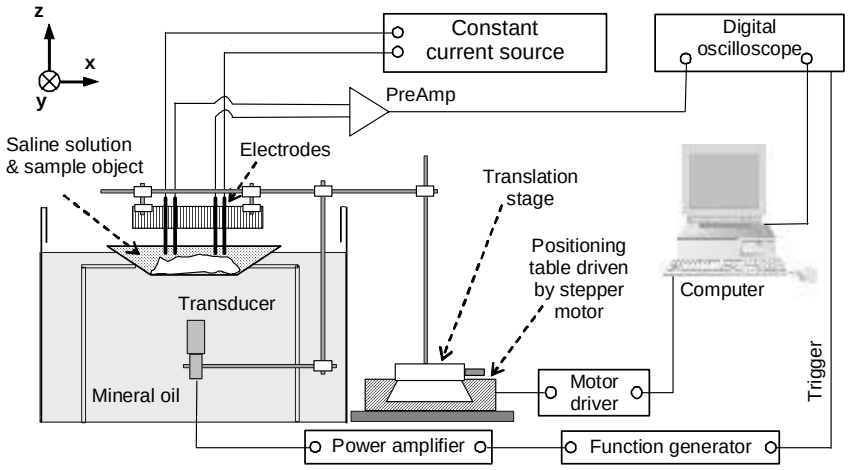

Figure 1 Schematic of the AET experimental system

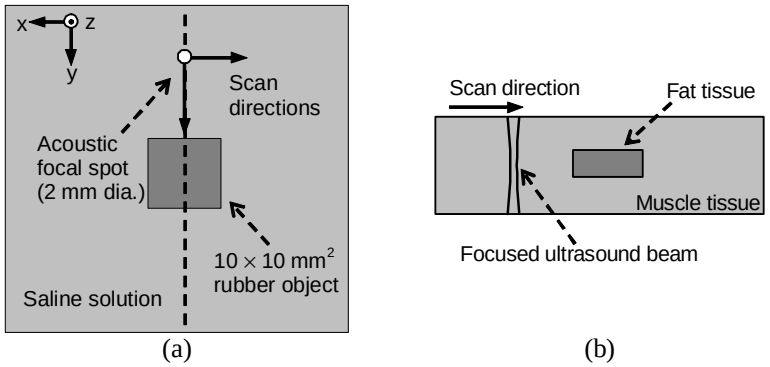

Figure 2 Cross sections of the saline-rubber phantom on (a) the *x-y* plane and (b) the *z-x* plane

2. METHOD

A schematic view of our experimental setup is shown in Fig. 1. An ultrasound transducer (VHP100-1-P38, Ultran Labs; central frequency: 1-MHz; focal length: 38 mm; focal zone: 20 mm; focal diameter: 2.1 mm) was located inside an imaging tank to transmit ultrasonic waves into a mineral oil bath. Mineral oil was used for acoustic coupling and electrical insulation. The transducer worked in a burst mode with 5 μs width and 100 Hz repetition rate. A function generator (DS345, Stanford Research System) generated the burst waves and system synchronizing trigger. The burst waves were amplified to 70 V (peak to peak) before being transmitted to the transducer. A four-electrode impedance-measuring system was used to detect the time-resolved AE modulation signals. The electrodes and the ultrasound transducer were raster scanned together in the *x-y* plane with a step size of 1.2 mm in both directions. A constant current source was employed in the experiment. A wide-band pre-amplifier (5662, Panametrics) amplified the detected AE modulations and was then AC coupled to a digital oscilloscope (TDS540, Tektronix). After averaging, the signals were finally transferred to the computer.

3. RESULTS AND DISCUSSION

We first imaged a saline-rubber phantom. Figure 2 describes its structure in two cross-sections. The sample container was made from polystyrene film (thickness: 0.3 mm). It was filled with a 0.9% saline (NaCl) solution to a depth of 20 mm. A natural gum rubber object (length: 10 mm; width: 10 mm; height: 5 mm) was placed at the center of the container where it did not touch either surface of the solution. The acoustic impedance of the natural gum matched that of the saline solution well.

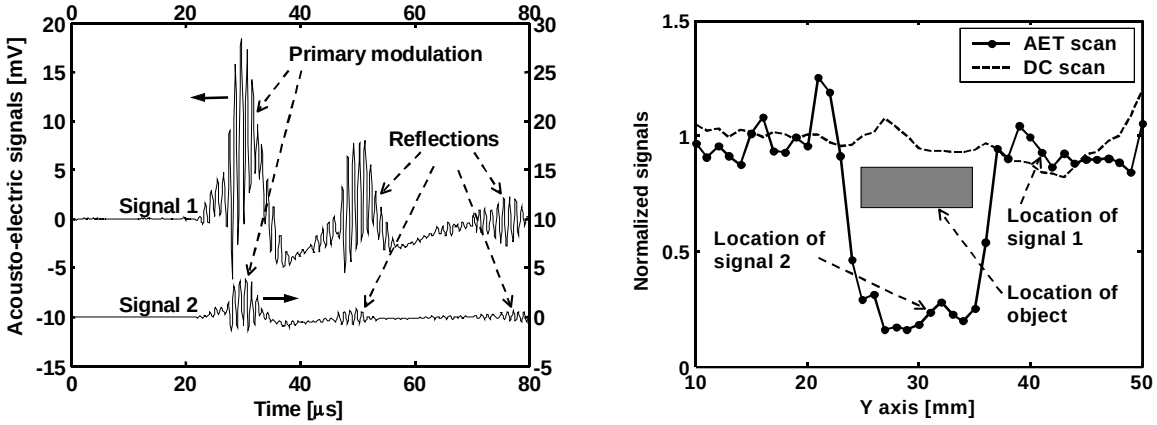

Figure 3 (a) The AE signals measured at different locations. (b) One-dimensional AET and DC scans of a saline-rubber phantom.

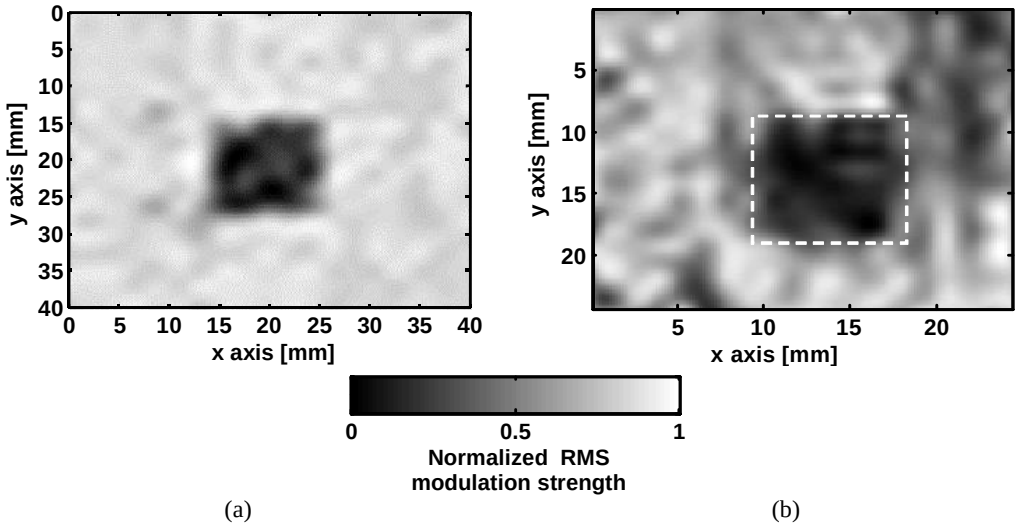

Figure 4 Two-dimensional AET images of (a) a saline-rubber phantom and (b) a tissue sample.

Figure 3(a) shows the AE modulation signals acquired from two locations in the phantom as marked in the one-dimensional (1D) AET image displayed in Fig. 3(b). Signal 1 was measured from a volume in the saline solution background and signal 2 was from a volume in the rubber occupied region. Because the conductivity of the saline solution was much higher than that of the rubber object, stronger modulation strength was observed in signal 1. Several studies were conducted to test the AE modulation signals. When the ultrasound emission was interrupted, the modulation signal disappeared. When the distance between the ultrasound transducer and the sample container was changed by a known value, the signal was observed to shift by an appropriate time period. When the driving voltage of the ultrasonic transducer increased linearly, the modulation strength was observed to increase by the same linear factor. Moreover, the spectral analysis of the detected AE signals showed good agreement with the 1-MHz central frequency of the applied

ultrasonic wave. Since the rubber object had a much lower conductivity than the surroundings, we observed weak AE modulations clearly at the corresponding locations in Fig. 3(b). The relative location and size of the rubber in the image are clearly resolved and well matched to those of the original phantom. But the 1D DC (a pure electric impedance scan with ultrasound emission interrupted) scan resolved nothing.

Two-dimensional images from both the saline-rubber phantom and the tissue sample are given in Fig. 4. The tissue sample was made in the same manner as described in Fig. 2, but the background medium was changed to chicken breast tissue, and the rubber object was replaced by a fat object. As the biological tissue was less homogeneous than the saline solution, heterogeneities within the buried object and the background tissue were observed in the image. Nevertheless, the fat object was clearly resolved.

System resolution was quantified experimentally on a new tissue sample. Two pieces of fat tissue and muscle tissue of the same size (length: 40 mm; width: 20 mm; height 15 mm) were put side by side to make an edge. An edge-spread function (ESF) was acquired from a 1D AET scan crossing this edge, and the LSF was deduced by taking the first derivative of the ESF. Using the full-width at half-maximum of the LSF as the system resolution, the resolution of our current AET system is 2.3 mm, which agrees with the size of the ultrasound focus. This resolution of AET is much better than that of EIT for comparable sample sizes. It is primarily determined by the focal size of the ultrasound, and, therefore, it can be further improved by changing the ultrasonic parameters.

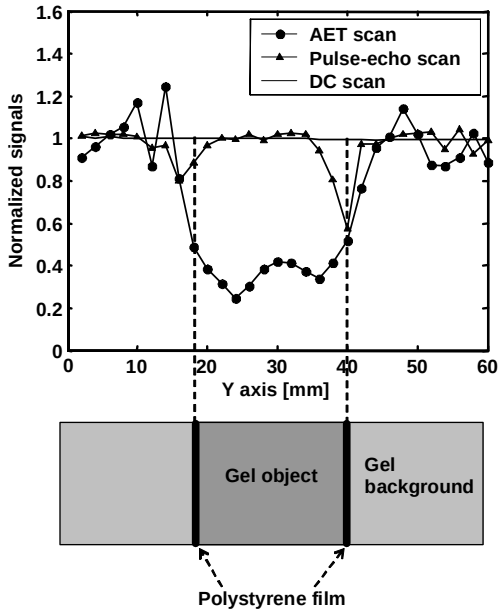

Figure 5 One-dimensional AET, pulse-echo, and DC scan results of a gel-gel phantom

The contrast mechanism of AET is demonstrated by studying a gel-gel phantom as shown in Fig. 5. The gel-gel phantom was made from two kinds of 8% g/ml gels (Gelatin, type A: from porcine skin, SIGMA, St. Louis, MO). The gel background (depth: 16 mm) was made using a 1% saline solution and the gel object (height: 16 mm; length: 22 mm; width: 22 mm) was made using distilled water. The gel object was further wrapped with polystyrene film on its 4 vertical walls and its top was covered by an ultrasonically transparent polyethylene membrane. The bottom side was left uncovered facing the incoming ultrasonic waves. The gel object was inserted at the center of the gel background as shown in Fig. 2(a). Except at the four vertical boundaries, there was no acoustic contrast. As constant electric current was applied, and due to the significantly lower conductivity of polystyrene and polyethylene, this wrapped gel object could be treated as an object with higher electric impedance relative to the gel background. Results from 1D AET, DC, and pure pulse-echo ultrasound scans were plotted together for comparison after normalization. Excluding the boundaries, almost no acoustic contrast was observed. But the AET scan resolved the whole object well. This confirms that AET is a means to image electrical impedance distributions even if ultrasonic contrast does not exist.

Unlike conventional ultrasonic imaging, AET is speckle-free. The reason is that acousto-electric signals, instead of back-scattered acoustic signals, are detected for imaging in AET. In other words, the mechanism for speckle formation in conventional ultrasonographic imaging does not exist in AET.

4. CONCLUSION

AET of saline-rubber phantoms and tissue samples were studied. Time-resolved AE modulation signals were detected, and two-dimensional AET images were acquired at 2.3 mm resolution. Results from the gel-gel phantom proved that the electric impedance contrast had been imaged. Higher resolution is possible if a finer focal size of the modulating ultrasound is employed. In conclusion, AET, based on direct image formation, is a powerful imaging method that combines the high contrast advantage of conventional EIT and the high resolution advantage of conventional ultrasonic imaging.

REFERENCES

1. Nycomed Amersham Intercontinental Continuing Education in Radiology, *The Encyclopaedia of Medical Imaging Volume I* (online version,) (http://www.amershamhealth.com/medcyclopaedia/Volume%20I/mammography.asp), 2002.
2. K. Kleiner, ″More gain, less pain - a new scanner could spare many women the trauma of a breast biopsy, ″ *New Scientist* 2184, pp. 16-16, 1999.
3. B. Brown and D. Barber, ″Applied potential tomography (APT) - a new in vivo medical imaging technique, ″ *Clinical Physics & Physiological Measurement* 4, pp. 96-96, 1983.
4. D. Barber and B. Brown, ″Applied potential tomography, ″ *Journal of Physics E: Scientific Instruments* 17, pp. 723-733, 1984.
5. A. Seagar, D. Barber, and B. Brown, ″Electrical impedance imaging, ″ *IEE Proceedings* 134, pp. 201-210, 1987.
6. T. Kerner, D. Williams, K. Osterman, F. Reiss, A. Hartov, and K. Paulsen, ″Electrical impedance imaging at multiple frequencies in phantoms, ″ *Physiological Measurement* 21, pp. 67-77, 2000.
7. A. D. Seagar, D. C. Barber, and B. H. Brown, ″Theoretical limits to sensitivity and resolution in impedance imaging, ″ *Clinical Physics & Physiological Measurement* 8, Suppl. A, pp. 13-31, 1987.
8. J. Jossinet, B. Lavandier, and D. Cathignol, ″The phenomenology of acousto-electric interaction signals in aqueous solutions of electrolytes, ″ *Ultrasonics* 36, pp. 607-613, 1998.
9. B. Lavandier, J. Jossinet, and D. Cathignol, ″Quantitative assessment of ultrasound-induced resistance change in saline solution, ″ *Medical & Biological Engineering & Computing* 38, pp. 150-155, 2000.
10. B. Lavandier, J. Jossinet, and D. Cathignol, ″Experimental measurement of the acousto-electric interaction signal in saline solution, ″ *Ultrasonics* 38, pp. 929-936, 2000.